

Small volume excitation and enhancement of dye fluorescence on a 2D photonic crystal surface

L. C. Estrada¹, O. E. Martínez¹, M. Brunstein², S. Bouchoule², L. Le-Gratiet²,
A. Talneau², I. Sagnes², P. Monnier², J. A. Levenson² and A. M. Yacomotti^{2,*}

¹Quantum Electronics Lab, Dpto. de Física. FCEN, Universidad de Buenos Aires, 1428, Buenos Aires, Argentina.

²Laboratoire de Photonique et de Nanostructures (CNRS UPR20), Route de Nozay, 91460 Marcoussis, France.

*Alejandro.Giacomotti@lpn.cnrs.fr

Abstract: We demonstrate an easy-to-implement scheme for fluorescence enhancement and observation volume reduction using photonic crystals (PhCs) as substrates for microscopy. By normal incidence coupling to slow 2D-PhC guided modes, a 65 fold enhancement in the excitation is achieved in the near field region (100 nm deep and 1 μm wide) of the resonant mode. Such large enhancement together with the high spatial resolution makes this device an excellent substrate for fluorescence microscopies.

©2010 Optical Society of America

OCIS codes: (180.1790) Confocal microscopy; (230.5298) Photonic crystals; (180.2520) Fluorescence microscopy; (180.4243) Near-field microscopy.

References and links

1. J. K. Jaiswal, and S. M. Simon, "Imaging single events at the cell membrane," *Nat. Chem. Biol.* **3**(2), 92–98 (2007).
2. S. W. Hell, and J. Wichmann, "Breaking the diffraction resolution limit by stimulated emission: stimulated-emission-depletion fluorescence microscopy," *Opt. Lett.* **19**(11), 780–782 (1994).
3. H. Rigneault, and P. Lenne, "Fluorescence correlation spectroscopy on a mirror," *J. Opt. Soc. Am. B* **20**(10), 2203 (2003).
4. M. F. García-Parajó, B. I. de Bakker, M. Koopman, A. Cambi, F. de Lange, C. G. Figdor, and N. F. van Hulst, "Near-Field Fluorescence Microscopy: An optical Nanotool to Study Protein Organization at the Cell Membrane," *NanoBiotechnology* **1**(1), 113–120 (2005).
5. M. J. Levene, J. Korlach, S. W. Turner, M. Foquet, H. G. Craighead, and W. W. Webb, "Zero-mode waveguides for single-molecule analysis at high concentrations," *Science* **299**(5607), 682–686 (2003).
6. J. R. Lakowicz, "Radiative decay engineering 5: metal-enhanced fluorescence and plasmon emission," *Anal. Biochem.* **337**(2), 171–194 (2005).
7. L. C. Estrada, P. F. Aramendía, and O. E. Martínez, "10000 times volume reduction for fluorescence correlation spectroscopy using nano-antennas," *Opt. Express* **16**(25), 20597–20602 (2008).
8. I. D. Block, P. C. Mathias, N. Ganesh, S. I. Jones, B. R. Dorvel, V. Chaudhery, L. O. Vodkin, R. Bashir, and B. T. Cunningham, "A detection instrument for enhanced-fluorescence and label-free imaging on photonic crystal surfaces," *Opt. Express* **17**(15), 13222–13235 (2009).
9. N. Ganesh, W. Zhang, P. C. Mathias, E. Chow, J. A. N. T. Soares, V. Malyarchuk, A. D. Smith, and B. T. Cunningham, "Enhanced fluorescence emission from quantum dots on a photonic crystal surface," *Nat. Nanotechnol.* **2**(8), 515–520 (2007).
10. L. C. Andreani, and D. Gerace, "Photonic-crystal slabs with a triangular lattice of triangular holes investigated using a guided-mode expansion method," *Phys. Rev. B* **73**(23), 235114 (2006).
11. X. Letartre, J. Mouette, J. L. Leclercq, P. R. Romeo, C. Seassal, and P. Viktorovitch, "Switching Devices With Spatial and Spectral Resolution Combining Photonic Crystal and MOEMS Structures," *J. Lightwave Technol.* **21**(7), 1691–1699 (2003).

1. Introduction

In recent years, many research activities were devoted to both enhancing the emission of fluorescent molecules and improving the spatial resolution of conventional far field microscopies. Increasing the intrinsic fluorescence of molecules is of great practical interest because it enhances the potential of molecular-fluorescence-based devices and techniques, whereas the reduction in the detection volume enables the observation of events (e.g. in living cells) at the single molecule level [1]. These methods include phenomena such as stimulated emission depletion [2], interference fringes in the excitation beam [3], near-field fluorescence

microscopy [4], zero-mode waveguides in nanoholes [5], and plasmon-based techniques using metallic films and nanoparticles [6], such as optical nanoantennas [7].

In this context, the techniques based on optical resonances in wavelength-scale periodic dielectric structures have gained importance for a wide range of applications (e.g. label-free sensing [8]). The guided-mode resonance in one and two-dimensional photonic crystal (PhC) slabs can ideally possess arbitrarily high quality factors, which are eventually limited by the (low) absorption of the dielectric material since scattering loss, due to fabrication imperfections, can be reduced by technological improvement. Moreover, compared to the plasmonics approach, photonic enhancement does not suffer from fluorescence quenching and/or lossy surface waves for very small distances between the fluorophore and the metal [6].

In previous works, enhanced fluorescence has been obtained as a result of both the near-field enhancement and coherent scattering from the PhC [9]. This was possible due to narrow angle resonances, making these substrates excellent sensors devices [8] but with poor lateral resolution for microscopy. Our goal in this work is to show an easy-to-implement scheme for fluorescence purposes with both axial and lateral confinement as well as fluorescence enhancement properties based on resonant excitation of slow 2D-PhC guided modes.

2. Photonic crystal design

In order to intensify and tightly confine light within a thin dielectric layer, a 2D-PhC has been designed. A light beam, normally incident with respect to the PhC periodicity [see Fig. 1(a)], may couple into the PhC slab through Bloch modes with zero (or near zero for a finite illumination spot) wavevector in the plane, i.e. the Γ point in the first Brillouin zone. Modes at the Γ point are in principle leaky, and the coupling strength of the guided to the radiative modes can be characterized through the coupling time τ_c , related to the quality factor through $Q = \omega\tau_c$. Modes with finite τ_c can be excited with a vertical beam, whereas modes with infinite τ_c —i.e. vanishing coupling strength because of symmetry reasons—are generally not accessible with external illumination. Furthermore, Bloch modes are well adapted for uniform substrate applications due to the small period-discrete translation invariance of the PhC lattice.

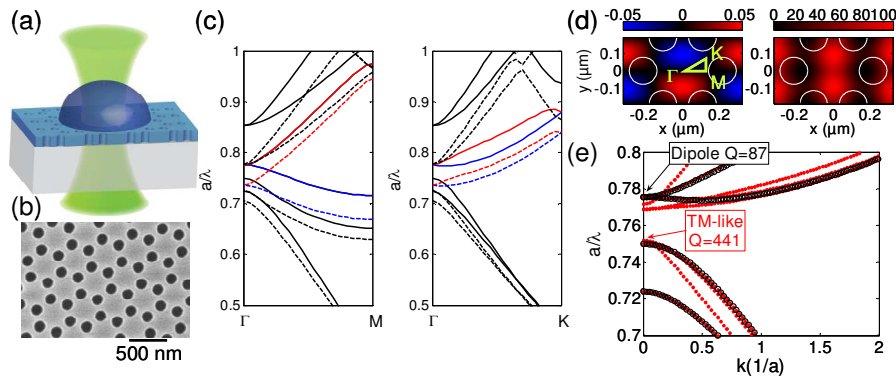


Fig. 1. (a) Dielectric photonic crystal slab with a water drop on top, illuminated by a tightly focused Gaussian beam in the visible. (b) SEM image of the fabricated SiN-PhC. (c) Band diagram for the fundamental TE guided mode in a graphite PhC in air with $a = 377.6$ nm and $d = 152$ nm. Dashed lines: water on top and inside the holes. Blue and red lines: dipole modes. (d) Hz (left) and energy density normalized to the one on the homogeneous slab (right) at the PhC/water interface, calculated with 3D-FDTD simulations of the periodic lattice under x-polarized plane wave injection at resonance. (e) Band calculation for both TE and TM fundamental guided modes (red dots) and for TE modes only (black circles) in air, along the Γ K direction. Only finite Q modes at the Γ point are highlighted with a text box.

Our structure is based on a 200 nm-thickness silicon nitride (SiN) slab on a silica substrate, which supports two guided modes at ~ 500 nm (TE and TM modes). The PhC geometry of our design is a graphite lattice of air holes [Fig. 1(b)]. The photonic band diagram was computed using a guided mode expansion technique, which allows the calculation of both

the frequency and the coupling times [10]. For simplicity, we first analyze the results considering the fundamental TE guided mode only [Fig. 1(c)]. Two bands (the red and blue bands) are degenerated at the Γ point at $a/\lambda = 0.7756$ for air as the top medium, and they have the same τ_c corresponding to $Q = 87.1$. Such modes are called “dipole modes” due to the two-lobe magnetic field profile on the plane [Fig. 1(d)]. The remaining two bands below the dipole modes (black bands in Fig. 1(c) with $a/\lambda = 0.75$ and $a/\lambda = 0.724$, known as the hexapole and monopole modes respectively) have infinite τ_c at the Γ point as a result of the odd symmetry of E_x and E_y components. Hence, they do not couple to the radiative modes.

Changing the air medium to water shifts the bands to a lower frequency due to the increase of refractive index [Fig. 1(c)]. The dipole modes at the Γ point shift to $a/\lambda = 0.7363$ (close to the target wavelength $\lambda = 514.5$ nm of our excitation laser), with $Q = 231.8$.

The band calculation for both TE and TM fundamental guided modes in air is shown in Fig. 1(e). Several TM-like bands are observed, out of which only two have finite coupling times at $a/\lambda = 0.752$ ($Q = 441$), hence they are potentially able to couple to vertical illumination.

One of the key issues in our design is to efficiently couple light into PhC modes in the case of a tightly focused beam on the sample, which are typical working conditions in confocal microscopy. Following reference [11], a sufficient condition for efficient coupling is

$$\delta\omega_d < \delta\omega_c \quad (1)$$

where $\delta\omega_d = |\omega(\mathbf{k}) - \omega(\mathbf{k} = 0)|$ is the spectral broadening due to the band dispersion within the illuminated region in k -space, and $\delta\omega_c = \tau_c^{-1}$ is the broadening due to radiative losses. Using Gaussian beams, condition (1) means that the radial propagation distance before diffraction out of the plane is smaller than the beam waist, i.e. photons do not escape laterally. We have computed condition (1) in k -space. As a result, the first dipole band in water can be efficiently coupled provided that $k_0 = 2/w_0 < 0.3/a$, i.e. a beam waist $w_0 > 2a/0.3 \sim 2.5$ μm [Fig. 2(a)], and $w_0 > 3.8$ μm for the second dipole band [Fig. 2(b)]. In addition, we verified that coupling to hexapole and monopole modes with vertical beams is inefficient with micrometer-sized w_0 .

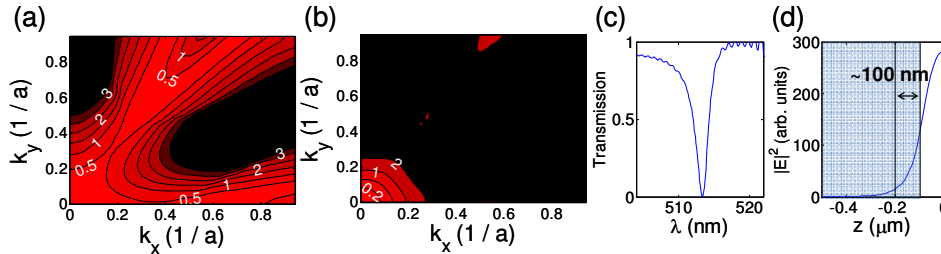


Fig. 2. Contour plot of $F(\mathbf{k}) = \delta\omega_d/\delta\omega_c$ in water for (a) the first dipole band and (b) second dipole band, showing efficient ($F < 1$, red) and inefficient ($F > 1$, dark) coupling regions. x (y) corresponds to ΓK (ΓM). (c) Transmission spectrum of the periodic graphite lattice calculated with FDTD simulations. (d) Intensity at $x = 0$ and $y = 0$ as a function of the vertical coordinate (z), showing the 100 nm-evanescent tail (blue region is water).

Finally, the transmission around 515 nm for the water/SiN/SiO₂ PhC slab was computed using 3D-Finite Differences Time Domain (FDTD) simulations for the periodic system under plane wave injection. The signature of the coupling to the dipole mode is a transmission dip [Fig. 2(c)] with almost 100% contrast centered at $\lambda = 513.4$ nm and with $Q = 224$. In resonance, the evanescent tail (to $1/e^2$ of the intensity at the interface) in the water is $\delta \sim 100$ nm [Fig. 2(d)].

3. Fabrication and characterization

A 200 nm layer of silicon nitride (Si_xN_y) is first deposited on a commercial fused silica substrate by plasma enhanced chemical vapor deposition. During the process, 8% of oxygen is incorporated into the Si_xN_y matrix in order to reduce the optical absorption in the visible. This

leads to a refractive index of 1.84 at $\lambda \sim 500$ nm (measured by ellipsometry), high enough to confine the optical mode. The PhC pattern is obtained using e-beam lithography on a 300 nm-thickness polymethyl methacrylate (PMMA) layer spin-coated on top of the SiN. The holes are finally transferred into the SiN layer through reactive ion etching. The PhC mask is a graphite array of holes inside a 200 μm -side square, with the following target parameters: lattice period $a = 377.6$ nm (218 nm between adjacent holes), and holes diameter $d = 152$ nm [Fig. 1(b)]. By varying the e-beam dose, the resulting diameters range from 107 to 156 nm.

In order to spectrally characterize the samples, white light transmission spectra were measured. A nonpolarized white light beam from a pulsed supercontinuum source (pulse duration ~ 1 -2 ns, repetition rate = 25 kHz) is focused on the sample. The waist diameter is 50 μm , the transmission is coupled into an optical fiber and finally detected with an optical spectrum analyzer. Spectra are normalized using the transmission signals outside the PhC, i.e. through the homogeneous SiN/silica layer. Measurements were performed on the bare samples as well as on the samples submerged into water. In the last case, normalization is given by the water/SiN/silica system. The results are shown in Fig. 3(a)-3(e). Note that as hole diameter is reduced, the spectral features (dips) red-shift and the distance between two dips decreases. Such red-shifts come from effective refractive index increase as holes shrink.

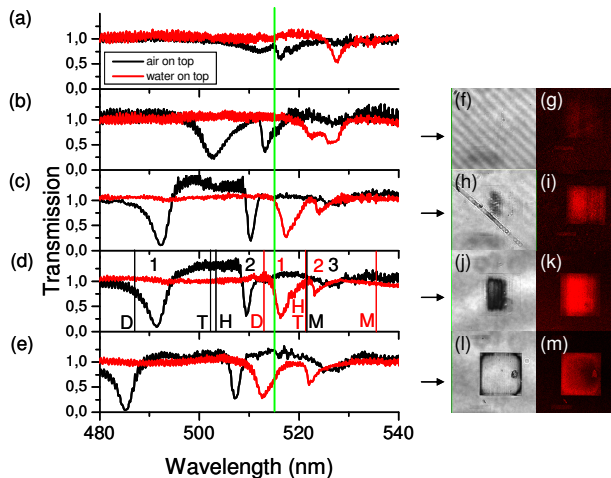


Fig. 3. (a)-(e) Transmission spectra for PhC structures with different holes diameters measured with (red line) and without (black line) water on the top: 133 nm (a), 139 nm (b), 148 nm (c), 152 nm (d) and 156 nm (e). Green line: the illumination wavelength in confocal experiments. (f)-(m) Transmission (left) and fluorescence (right) images recorded by raster-scanning over the PhC.

Hole diameters in Fig. 3(d) are $d = 152$ nm, corresponding to the parameters of Sec. 2. In air, two well-contrasted transmission dips [labeled “1” and “2” in Fig. 3(d)] can be identified: a wide dip “1” at $\lambda \approx 491$ nm and narrower one “2” at $\lambda \approx 509$ nm. Band calculations from Sec. 2 give the expected wavelengths of the following Bloch modes at the Γ point: the dipole (D), finite Q-TM-like (T), hexapole (H) and monopole (M) modes. Dip “1” is close to the D mode, and dip “2” is close to the T and H modes. A third dip with small contrast (“3”) can also be observed at $\lambda \approx 527$ nm, which could be related to mode M. In summary, the two modes that are expected to couple because of finite Q (dipole and TM-like modes) are close to the two resonances with highest contrasts (“1” and “2”).

In the case of samples in water, the dip “1” is red-shifted to $\lambda \approx 516$ nm, i.e. for about 25 nm with respect to the in-air counterpart. Dips “1” and “2” are also close to modes D and T in water. This constitutes evidence that water is indeed filling the holes. Further calculations show that in the case of water not filling them, i.e. just remaining on top, the expected shifts are about 3 nm. The slight differences –less than 1%– between the theoretical predictions and the observed wavelengths are within the error bars in the measurements of refractive index

and hole diameters. Finally, the experimental Q-factors are $Q_{D,air} = 112$ and $Q_{D,water} = 143$ for the dipole mode; the theoretical values were 87 and 232 respectively. For the TM-like mode we obtain $Q_{T,air} = 335$, whereas the band calculation gives 441. Discrepancies between theory and experiment can be attributed to the lack of finite lateral size effects in the calculation and errors in the experimental Q-factors obtained from the FWHM of the resonances.

4. Confocal microscopy studies

The PhC was used as a substrate to enhance the excitation of molecules. Fluorescence measurements were performed on a commercial inverted confocal microscope (Olympus FV1000). The setup is shown in Fig. 4(a). The excitation light (the 514.5 nm line of a linearly polarized Argon laser) is focused to a $\sim 1 \mu\text{m}$ spot onto the PhC-fluorescent sample interface using a 10X, NA = 0.4 objective. The fluorescence is collected by the same objective and separated from the excitation light by a dichroic mirror. A pinhole rejects out of focus light. The signal is sent onto a photomultiplier through a 555–655 nm bandpass filter.

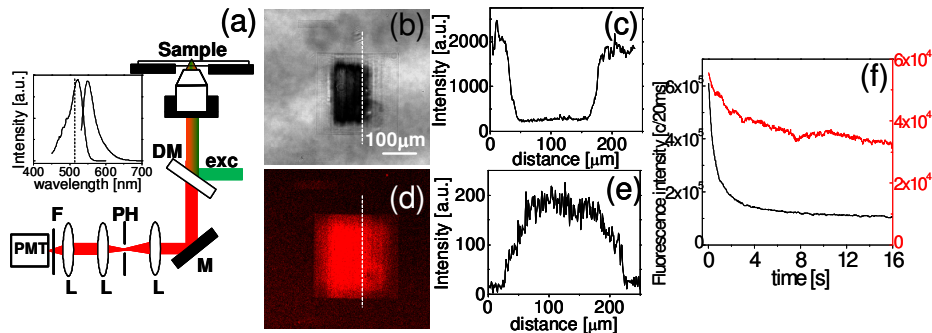


Fig. 4. (a) Sketch of a confocal microscope. The excitation light is focused onto the PhC. The focal spot is imaged onto the detector via a pinhole. DM: dichroic mirror, M: mirror, L: lens, PH: pinhole, F: filter, PMT: photomultiplier. Inset: R6G/water absorption and emission spectra, showing that the R6G absorbs the excitation laser. Single raster-scan lineouts for transmission (b) and fluorescence (d) confocal images recorded simultaneously by raster scanning a solution of 1.5 μM R6G/water over the PhC. The emission of molecules is enhanced due to the PhC-resonant excitation. (c), (e) Intensity profiles as a function of position along dashed lines in (b) and (d). (f) Fluorescence intensity for a drop of Rhodamine 6G/water solution over a PhC when a single point is irradiated with 70 μW . On the PhC surface (black) and off the PhC surface (red).

Figures 4(b) and 4(d) show transmission and fluorescence confocal images recorded simultaneously by raster-scanning a sample of 1.5 μM Rhodamine 6G (R6G) (Exciton) in water solution over a PhC slab. The dark region in Fig. 4(b) corresponds to the decrease of transmitted intensity down to 10% of its maximum [see Fig. 4(c)]. Remarkably, this high contrast with 1 μm -spot overcomes what was expected from the theoretical estimation of w_0 given in Sec. 2; theoretical simulations including finite-size effects are needed for further understanding the dependence of coupling on the waist size. We also point out that changing the excitation wavelength to 488 nm, the dark region disappears, since the excitation is no longer in resonance. Fig. 4(d) clearly shows a significant PhC-fluorescence enhancement (\mathfrak{F}), which is obtained from Fig. 4(e) as the ratio between the signal inside, S_{in} , and outside, S_{out} , the PhC structure, and gives $\mathfrak{F} \sim 10$. Note that \mathfrak{F} extends over the same dark region of Fig. 4(b).

In order to further investigate the resonant character of the excitation, we relate the confocal images to the spectral features obtained in Section 3. This is summarized in Fig. 3. For $d = 156 \text{ nm}$ [Fig. 3(e), 3l-m], transmission and fluorescence are only modified close to the PhC boundaries. Indeed, since the excitation is red-detuned with respect to the resonance inside the PhC (peak “1” in water), we can expect resonant modes at the boundaries to approach the excitation wavelength due to the fact that holes are smaller close to the borders.

In Figs. 3(d), 3(j)-3(k) ($d = 152$ nm) the excitation is blue-detuned with respect to the resonance, but remains close to its minimum. Therefore, as it is expected, the fluorescence enhancement is stronger. It can also be observed that transmission contrast and fluorescence enhancement decrease for smaller air-holes in Figs. 3(h)-3(i), and almost extinguish in Fig. 3(f)-3(g).

5. Discussion

In this Section we interpret our results on fluorescence enhancement in terms of both confinement and enhancement of the excitation. Under confocal detection and PhC resonance conditions, two different volumes can be identified. One is defined by the diffracting focused beam and the confocal detection, $V_0 = A\delta'$, where δ' is an effective length given by $\pi^{1/2}\omega_z$, ω_z being the $1/e^2$ Gaussian width of the observation volume in the axial direction and A the illumination spot area. The second volume is the PhC-resonant mode region $v_0 \approx A\delta$, where δ is the evanescent tail of the mode penetrating in the aqueous medium. Assuming two populations of fluorescent molecules at time t , one adsorbed on the SiN surface with surface concentration $\rho(t)$, and one freely diffusing through the sample with volume concentration $C(t)$, the collected fluorescence signal outside and inside the PhC can be written as

$$S_{out}(t) = I_0 A \sigma_{abs} [\rho(t) + C(t) \delta' / 2] \quad (2)$$

$$S_{in}(t) = \eta I_0 A \sigma_{abs} [\rho(t) + C(t) \delta] + T I_0 A \sigma_{abs} C(t) \delta' / 2 \quad (3)$$

where I_0 is the excitation laser intensity, σ_{abs} is the absorption cross section of the molecules, η is the excitation enhancement factor and T the optical transmission at resonance. Assuming that $T\delta'/2 \ll \eta\delta$, the last term of Eq. (3) can be neglected, meaning that fluorescence output from molecules on top of the PhC essentially comes from a confined volume of depth δ . Figure 4(f) shows the fluorescence intensity time evolution upon single point irradiation during 16 seconds using $70 \mu\text{W}$. The curve shows a clear intensity reduction and no evidence of discrete steps caused by bleaching of individual molecules. At the beginning of the irradiation the fluorescence enhancement is $\mathfrak{F}_0 = S_{in}(0)/S_{out}(0) = \eta[\rho(0)/C(0) + \delta]/[\rho(0)/C(0) + \delta'/2] \approx 10$, in good agreement with the observation of Sec. 3. Due to the bleaching, after a few seconds, the contribution of adsorbed molecules can be neglected, i.e. $\rho(\infty) \sim 0$. As a result, the fluorescence enhancement after bleaching yields $\mathfrak{F}_\infty = S_{in}(\infty)/S_{out}(\infty) = 2\eta\delta/\delta' \approx 3$, which corresponds, in our conditions ($\delta \approx 0.1 \mu\text{m}$ and $\delta' \approx 4.4 \mu\text{m}$), to an excitation enhancement factor of $\eta \sim 65$.

Clearly, the observed difference between the fluorescence enhancement before, \mathfrak{F}_0 , and after bleaching, \mathfrak{F}_∞ , comes from a non negligible surface concentration. The ratio $\rho(0)/C(0)$ can thus be obtained and gives ~ 280 nm, hence $\rho(0) \sim 250$ molecules/ μm^2 for a $1.5 \mu\text{M}$ sample concentration. It is also interesting to note that in the limit $\rho/C \rightarrow \infty$ (dry sample), the fluorescence enhancement is expected to attain its maximum given by η . The factor $\eta \sim 65$ can be compared to the numerical simulations. The energy distribution of the dipole mode [Fig. 1(d)] shows pairs of hot spots located inside the hexagonal cell of holes, with maxima of about 110 times the energy over the homogeneous slab. The averaged energy on the plane gives $\eta \sim 50$, in very good agreement with the experimental result. The small difference may be due to the intensification inside the holes, which has been neglected in this calculation.

6. Conclusions

Through resonant excitation of a PhC leaky mode, a 65-fold near field excitation enhancement of R6G in water on a SiN-based 2D-PhC surface was demonstrated. Under normal incidence illumination, the observation volume is confined both in the lateral ($1 \mu\text{m}$, defined by the high localization of slow modes), and axial (100 nm thickness, defined by the evanescent field penetrating the fluorescent solution) directions. Thus, our PhC substrates give a handle to

improve spatial resolution under pointwise excitation conditions using commercial confocal microscopes, with potential interest in the detection of localized events in cellular membranes.

Acknowledgments

L. Estrada is a doctoral fellow from CONICET. These results are within the scope of C'Nano IdF and were supported by the Région Ile-de-France. C'Nano IdF is a CNRS, CEA, MESR and Région Ile-de-France Nanosciences Competence Center.